The Astrophysical Journal, 785:6 (7pp), 2014 April 10 doi:10.1088/0004-637X/785/1/6

NUCLEATION AND STABILIZATION OF CARBON-RICH STRUCTURES IN INTERSTELLAR MEDIA

N. Patra[1,3], P. Král[1,2], and H. R. Sadeghpour[3]
[1] Department of Chemistry, University of Illinois at Chicago, Chicago, IL 60607, USA; npatra2@uic.edu
[2] Department of Physics, University of Illinois at Chicago, Chicago, IL 60607, USA; pkral@uic.edu
[3] ITAMP, Harvard-Smithsonian Center for Astrophysics, Cambridge, MA 02138, USA; hrs@cfa.harvard.edu
Received 2013 December 26; accepted 2014 February 2; published 2014 March 21

ABSTRACT

We study the conditions under which carbon clusters of different sizes form and stabilize. We describe the approach to equilibrium by simulating tenuous carbon gas dynamics to long times. First, we use reactive molecular dynamics simulations to describe the nucleation of long chains, large clusters, and complex cage structures in carbon- and hydrogen-rich interstellar gas phases. We study how temperature, particle density, the presence of hydrogen, and carbon inflow affect the nucleation of molecular moieties with different characteristics, in accordance with astrophysical conditions. We extend the simulations to densities that are orders of magnitude lower than current laboratory densities, to temperatures that are relevant to circumstellar environments of planetary nebulae, and microsecond formation times. We correlate cluster size distributions from the simulations with thermodynamic equilibrium at low temperatures and gas densities, where entropy plays a significant role.

Key words: astrobiology – astrochemistry – infrared: ISM – ISM: molecules – planetary nebulae: general – methods: numerical – molecular processes

Online-only material: color figures

1. INTRODUCTION

Carbon-based chemistry of the interstellar medium (ISM) is now an established discipline. The presence of a large variety of organic molecules such as aldehydes (Marcelino et al. 2007), alcohols (Friberg et al. 1988; Marcelino et al. 2007), ethers (Garrod & Herbst 2006), amides (Hollis et al. 2006), sugars (Hollis et al. 2000), acids (Garrod & Herbst 2006; Gibb et al. 2004), amino acids (Botta & Bada 2002; Cronin & Chang 1993), and nitriles (Belloche et al. 2008), as well as many long-chain hydrocarbon compounds in the dense ISM has been confirmed by infrared, radio, millimeter, and submillimeter spectroscopic measurements (Irvine et al. 1987; Ohishi & Kaifu 1998; Winnewisser & Kramer 1999; Schutte 1996; Herbst & van Dishoeck 2009; Hollis et al. 2000). The detection of ring species, including aromatic rings, raises the possibility that biologically significant molecules may exist in the ISM. Between 10%–30% of the interstellar carbon budget is thought to reside in polycyclic aromatic hydrocarbons (PAHs; Tielens 2008).

The presence of complex molecules, with typical spectral properties, can be used to precisely probe the environments in which they reside and provide a fairly accurate history of ISM molecular clouds. IR emission lines (in the range of 3–14 μm) have been assigned to C–C and C–H vibration bands of a broad class of PAHs (Salama 2008; Ehrenfreund & Sephton 2006; Duley 2006; Salama et al. 1999; Ricks et al. 2009; Herbst & van Dishoeck 2009; Tielens 2008). The simplest PAH, naphthalene ($C_{10}H_8$), has been found in carbonaceous chondrites (Spencer et al. 2008), suggesting extraterrestrial origin. Although no specific PAH molecule has been unambiguously identified in space, infrared emission bands have been observed in nearly all astronomical objects, from highly ionized H II regions to ultraluminous infrared galaxies.

The emission features at 7.0, 8.5, 17.4, and 18.9 μm, which are present in the spectra of the planetary nebula, Tc1, and the reflection nebulae, NGC 7023 and NGC 2023, have been conclusively associated with the vibrational lines of regular carbon cages (C_{60} and C_{70}) (Cami et al. 2010; Sellgren et al. 2010). Moreover, a large class of unsolved mysteries in astronomy, such as diffuse interstellar bands (DIB; Allamandolla et al. 1985), extended red emission (ERE; Witt & Schild 1984), and the 2175 Å "bump" (Bradley et al. 2005), trace their origins to large carbon and/or carbonaceous molecules. Single- and multilayer graphene have strong plasmon excitation bumps in the vicinity of the 2175 Å feature (Eberlein et al. 2008). However, more work is needed to establish a potential connection between these spectral features in astrophysical conditions. These challenges cannot be solved without strong theoretical input. The development of comprehensive and detailed theoretical models for the origin and evolution of complex organic molecules such as PAHs, fullerenes, and other ordered carbon structures may be crucially important for understanding the role of prebiotic molecules on early Earth.

Most theoretical studies of the formation of larger aromatic carbon chains, rings, and cages in ISM have been performed close to equilibrium and at relatively high particle densities. Naphthalene ($C_{10}H_8$) was shown to have potentially formed in ISM via a barrierless reaction between phenyl radical (C_6H_5) and vinylacetylene (C_4H_4; Parker et al. 2012). It was proposed that C_{60} in ISM can form in a top-down manner through the successive de-hydrogenation of PAHs into graphene (Berné & Tielens 2012), and the formation of defects (pentagons) necessary for the synthesis of C_{60}. However, there are a number of issues associated with this hypothesis. (1) The circumstellar environment of the Tc1 planetary nebula is distinctly hydrogen poor, (2) graphene is only synthesized in the laboratory and is not believed to exist in ISM, and (3) the proposed formation of carbon cages in ISM (via the six- to five-member rings) was only observed in the laboratory in conditions that were far from equilibrium.

To our knowledge, there are no available dynamical simulations that demonstrate the formation of molecules with aromatic rings in astrophysically relevant conditions, which are not properly known. The orderly growth of planar carbon structures

(hexagon rings) from precursor C_2 molecules necessitates low-temperature conditions, where vibrational distortions of the structures are minimized during their growth (Irle et al. 2003). Under such conditions, no significantly curved (cage-like) structures are supposed to form (Irle et al. 2003). Higher temperatures or a faster inflow of carbon material is needed to form curved carbon clusters and fullerenes (pentagon rings, ring-stacks, and ring fusion). In the laboratory, fullerenes are created with remarkable efficiency (≈40% in a condensing carbon arc) under less understood conditions far from equilibrium.

In this work, we describe the approach to equilibrium by simulating tenuous carbon (and hydrogen) gas dynamics over a long period of time. The different carbon molecular clusters and moieties that form represent steady-state, local equilibria and are important gauges for understanding future time dynamics and equilibration in astrophysical time.

2. SIMULATIONS OF CLUSTER GROWTH

We aim to understand the nucleation and stabilization of carbon chains, rings, and cages of different sizes, and moieties in regimes relevant to astrophysics (cold temperatures and low densities), which are orders of magnitude more dilute than those considered under laboratory conditions (Irle et al. 2003, 2006). However, performing such simulations in gaseous conditions resembling an ISM is a highly challenging task. Since the cluster formation times are long and the systems are large, we cannot reasonably investigate them using first principle molecular dynamics (MD) methods unless we only focus on equilibrium structures; for example, fullerene forms caused by laser irradiation or arc-discharge methods within 1 ms to several seconds. By increasing the density of carbon atoms, we can effectively compress the nucleation time. However, this time compression dramatically alters the entropic contribution to the cluster Gibbs energy and thus influences the cluster form and stability.

Here, we use semi-classical reactive MD simulations to model the formation of clusters starting from an elementary carbon (and hydrogen) gas. To proceed with the simulations, we need to know the reactive force fields, characterized by appropriate potential functions describing the change of atom hybridization over time. We use an approximate description of the chemical bonds and propose analytical fit formulae for the structure formation times.

We apply the adaptive intermolecular reactive empirical bond-order (AIREBO) potential function proposed by Stuart (Stuart et al. 2000), based on the Brenner bond-order potential (Brenner 1990). This potential can be used for chemical reactions and intermolecular interactions in condensed-phase hydrocarbon systems such as liquids, graphite, and polymers. The potential function is given by

$$E_{\rm Total} = E_{\rm REBO} + E_{\rm LJ} + E_{\rm tors},$$
$$E_{\rm REBO} = V_{ij}^{R}(r_{ij}) + b_{ij} V_{ij}^{A}(r_{ij}), \quad (1)$$

where V_{ij}^{R} and V_{ij}^{A} are repulsive and attractive pairwise potentials between atoms i and j, separated by r_{ij}, and b_{ij} is the bond-order term in a Tersoff-type potential (Stuart et al. 2000). The dispersion and intermolecular interactions ($E_{\rm LJ}$) are modeled with a Lennard–Jones (LJ) 12–6 potential, having a switching function and a connectivity switch (Stuart et al. 2000). The torsional potential ($E_{\rm tors}$) is proportional to bond weights that contribute to the dihedral angle (Stuart et al. 2000).

We model the self-assembly of clusters from C and/or H atom gases using atomistic reactive MD simulations with the AIREBO potential (Stuart et al. 2000) as implemented in the LAMMPS package (Plimpton 1995). The systems are modeled in the canonical (NVT) ensemble with periodic boundary conditions applied. The Langevin damping method (Servantie & Gaspard 2003), with a damping coefficient of 0.01 ps^{-1}, is used to thermalize the systems; the time step is 0.5 fs. Visualization and analysis of the trajectories were performed with visual MD software (Humphrey et al. 1996).

As temperatures increase, the simulations progressively become more computationally expensive and finer time steps are required (scaling is linear with temperature). For instance, it takes 24 hr to simulate 10,000 C atoms at $T = 3000$ K for a $t \approx 1$ ns simulation time on a 120 core machine with 2.6 GHz AMD Opteron processors. For the same reason, higher temperature ($T = 2000$ K) systems are simulated for up to $t = 50$ ns.

3. RESULTS AND DISCUSSION

Evidence from theoretical studies suggests that high temperatures are required to transform a flat structure into a curved moiety (Lozovik & Popov 1997). In our simulations, we examine the type of structures that are formed at different temperatures and gas densities.

3.1. Nucleation of Carbon Clusters at Different Temperatures and Densities

First, we simulate the nucleation of carbon clusters at different temperatures ($T = 300$–3000 K). We place 512 atoms in a box of $50 \times 50 \times 50$ nm^3, giving a carbon particle density of 4.1×10^{-6} $Å^{-3}$. In the MD simulations, the system energy is first minimized for a short time (5 ps). In most implementations of the MD algorithm, which is applicable to high density gases and biological complexes, the system is initially relaxed to a minimum energy to avoid unnecessary coordinate overlaps or collisions. While this initial minimization is not necessary in our simulations, due to low densities, we maintain it for a very short period. Then, the systems are heated to the target temperature and simulated for up to 3 μs.

In Figure 1, we present snapshots of the carbon moieties formed at different temperatures and times. At $T = 3000$ K, clusters appear at much earlier times because the diffusion and collision rates are faster. The high thermal energy also helps to induce curvature in the flat structures at much earlier times. As shown in Figure 1 (top panel), (a) planar clusters form within $t = 10$ ns and (b) large planar clusters with five and six member rings emerge after $t = 25$ ns, while (c) fully formed fullerene structures (C_{70}–C_{84}) appear after $t = 50$ ns. Even at early times, defects (pentagons) are present in the moieties, heralding the process of curvature formation. After $t = 90$ ns, nearly all structures are cages. In our simulations, for small systems, all carbon atoms form curved structures, but in a much bigger system at the same density and at high temperature, predominantly smaller carbon clusters form along with a few planar and curved moieties when the system is in or close to equilibrium (see distribution of cluster sizes section).

At $T = 2000$ K, the temperature is still high enough to overcome the transition barriers (from flat structures to curved structures). Snapshots at $t = 25$, 50, and 75 ns (d–f) are provided in Figure 1. The existence of five-member rings at $t = 25$ ns (d) is a prelude to a cage-like structure formation. At $t = 50$ ns

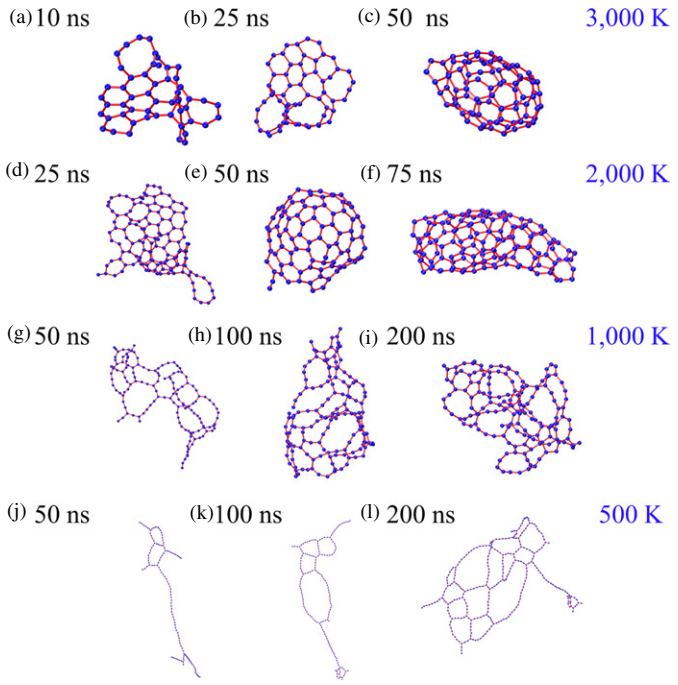

Figure 1. Nucleation of carbon clusters at different temperatures, T ((a–c) $T = 3000$ K; typical structures are shown). (a) Formation of planar clusters (six-member rings) is observed within 10 ns. (b) Fullerene-type and big planar clusters, with six- and five-member rings, are observed after $t = 25$ ns. (c) Almost all carbon atoms form fullerene-type clusters (C_{70}–C_{84}) within $t = 50$ ns. ((d–e) $T = 2000$ K). (d) Planar structures are formed within $t = 25$ ns. (e) Formation of cage-like structures with five- and six-member rings observed after $t = 50$ ns. (f) Cylindrical clusters, due to the merger of small fullerene-type clusters, are found within $t = 75$ ns. ((g–i) $T = 1000$ K). (g) Long chains emerge from short chains and eventually large member ring structures are observed (snapshot taken at $t = 50$ ns). (h) Several large member rings form cage-like structures (snapshot taken at $t = 100$ ns). (i) Formation of five- and six-member rings is observed after $t = 200$ ns. ((j–l) $T = 500$ K). (j) Long chain molecules are observed within $t = 50$ ns. (k) Large member rings emerge from long chains after $t = 100$ ns. (l) Planar clusters with big rings are found after $t = 200$ ns.

(A color version of this figure is available in the online journal.)

(e), curvature is dramatic and a fullerene-like structure begins to form. At $t = 75$ ns (f), cylindrical nano-structures emerge due to the merger of fullerene-type clusters. Again, at $T = 2000$ K, the high thermal energy hinders the formation of large clusters and small clusters are more likely to be present in equilibrium (see the distribution of cluster sizes section).

As we decrease the temperature, large clusters can be stabilized, as shown in Figures 1(g)–(i). At $T = 1000$ K, though defects form after a short period of time, $t = 50$ ns (g), chain-like structures tend to form,, while cage-like structures begin to appear after $t = 100$ ns (h). At $t = 200$ ns (i), curvature is clearly evident, though the regularity of the type present at higher temperatures is lacking.

Long chains can be stabilized at lower temperatures. Snapshots at $t = 50, 100$, and 200 ns (j–l) in the lower panel of Figure 1, illustrate that chain formation is readily accomplished at $T = 500$ K with instances of several irregularly formed rings. At $T = 500$ K, the cage-like formation occurs after a very long period of time, if at all. At $t = 200$ ns (l), there is evidence of curvature formation, but rings that have odd-numbers of atoms are quite irregular in shape. For a much bigger system, carbon atoms can form several large clusters and a "liquid" phase at lower temperatures (see Section 3.3).

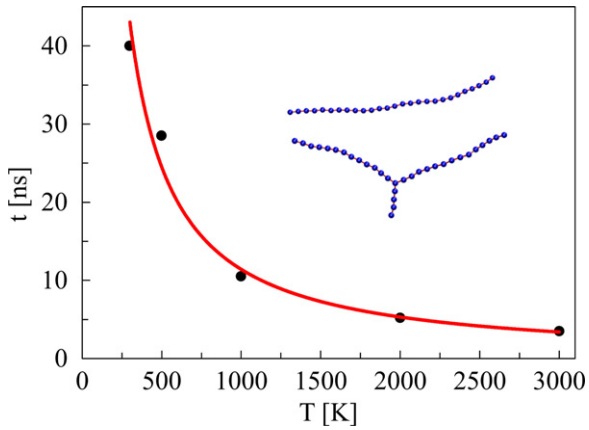

Figure 2. Nucleation time of small linear or branched carbon chains (inset: linear and branched carbon chains consist of $n_C \approx 30$ atoms) at different temperatures. The analytic dependence is $t(\text{ns}) = 23{,}153\, T^{-1.10}(\text{K})$.

(A color version of this figure is available in the online journal.)

While the formation of structures at much lower temperatures and densities is hampered by slow diffusion and collision rates, it is still possible to glean valuable information under these conditions by investigating the patterns that are present at higher temperatures and densities. We calculated the time taken to form a small linear or branched chain, with a carbon atom number, ($n_C \approx 30$), at different temperatures. As shown in Figure 2, at $T = 300$ K, small chains form after $t \approx 40$ ns, whereas at $T = 3000$ K, it takes $t \approx 3.5$ ns to form. The formation time at 500, 1000, and 2000 K, are 28.5, 10.5, and 5.2 ns, respectively. The analytic dependence between the time (t) and the temperature (T) is $t(\text{ns}) = 23{,}153\, T^{-1.10}(\text{K})$.

Next, we measured the time of formation of small graphene flakes at different temperatures. We observed graphene flakes after ≈9.7 ns at $T = 3000$ K, whereas at $T = 1750$ K, we noticed the formation of graphene flakes after $t = 18.4$ ns. We did not observe the formation of graphene flakes at $T < 1500$ K, which is likely due to the existence of a barrier below $T < 1750$ K. It is therefore possible to obtain a fit of the formation time vs. temperature. The analytical form is $t(\text{ns}) = 339{,}404\, T^{-1.31}(\text{K})$. This fit predicts that a graphene flake, assuming that the classical over the barrier can be penetrated, would form after $t(\text{ns}) \sim 193$ at $T = 300$ K.

Next, we study the effect of particle (carbon atom) density on the structure of carbon cages/clusters by placing 512 carbons atoms in the gas phase in a cubic box with periodic boundary conditions. The density of carbon atoms was changed (4.1×10^{-10}–5.8×10^{-7} Å^{-3}) by varying the box size at $T = 3000$ K. When the concentration is 5.8×10^{-10} Å^{-3}, we find only very short carbon chain molecules ($n < 10$) after $t = 450$ ns; no planar and fullerene-type clusters are observed. However, when we increase the concentration of carbon atoms ($\rho = 5.1 \times 10^{-7}$ Å^{-3}), short chain molecules emerge after $t = 100$ ns. After $t = 450$ ns, long chain molecules with few cage-like clusters are observed. Fullerene-type clusters are observed after 1 μs. Interestingly, no graphene flakes formed at $T = 3000$ K. However, they are observed after $t = 97$ ns and $t = 125$ ns at $T = 2500$ K and $T = 2000$ K, respectively. No graphene flakes are observed at $T = 300$ K and $T = 500$ K after $t \approx 3\,\mu$s. It should be mentioned that while our lowest density only extends down to $\approx 10^{14}$ cm^{-3}, many orders of magnitude more dense than typical interstellar cloud densities

of 10^4 cm^{-3}, our simulations and scaling dependencies are reflective of arbitrarily low temperature and density conditions.

3.2. Conditions at Chemical Equilibrium

The Gibbs free energy of any system can be written as

$$G = H - TS, \quad S = \frac{U}{T} + k \ln Q, \tag{2}$$

where H and S are the system's enthalpy and entropy, U and Q are its internal energy and a canonical partition function, and k is the Boltzmann constant, respectively. Using a molecular partition function, $q_{\rm tot}$, Q can be written as

$$Q = \frac{q_{\rm tot}^N}{N!}, \quad q_{\rm tot} = q_t\, q_r\, q_v\, q_e. \tag{3}$$

Here, N is the number of particles, q_t, q_r, q_v, and q_e are the translational, rotational, vibrational, and electronic partition functions. Using the partition functions, one can calculate the free energy of a gas at a particular temperature and volume. The competition between the entropy and enthalpy of the system determines the formation probability of a particular cluster as the system approaches equilibrium.

Under equilibrium conditions, the free energy of one mole of C_2 molecules (G_{C_2}) is equal to the free energy of two moles of isolated carbon atoms (G_{2C}), $G_{2C} = G_{C_2}$. The symmetry numbers (σ) for a diatomic molecule and the C–C bond distance are 2 and 1.54 Å, respectively. The bond energy (H_{C-C}) and the vibrational frequency (ν) of C–C are $\epsilon_D = 348$ kJ mol^{-1} (29090 cm^{-1}) and 1200 cm^{-1}, respectively.

The equilibrium constant for each mole of the reaction $C_2 \rightarrow 2C$ is defined as the ratio of partition functions, $k_p = ((q_C/N_A)^2/(q_{C_2}/N_A))e^{-\beta\epsilon_D}$, where the partition functions $q_C = q_t$, $q_{C_2} = q_t\, q_r\, q_v$ and N_A is the Avogadro's number (Laidler et al. 2003). For the C–C bond energy of ϵ_D, in ideal gas conditions, one obtains a constant $k_p = 5.4 \times 10^{-33}$ at $T = 500$ K, and a volume of dissociation equivalent to 2.6×10^6 m^3 per molecule. The immediate implication is that at low density equilibrium, only high entropy structures, such as filaments and small clusters, survive.

3.3. Size Distributions of Carbon Clusters

The carbon structures that form in simulations can have varying distributions according to atom size, moiety, ring size (pentagon, hexagon), and bond length, depending on the density and temperature of the gas. There can be large variations among the different clusters that form. We determined the probability distributions of structure size (C atom number) at different temperatures and densities by simulating two systems with 4100 and 10,000 carbon atoms (carbon density, $\rho = 4.0 \times 10^{-6}$ Å^{-3}, was the same in both systems) in gas phases at $T = 3000$, 2000, 1000, and 500 K. At $T = 500$ K, the size distribution is obtained after $t = 200$ ns. Similarly, for $T = 1000$, 2000, and 3000 K, the size distributions are obtained after $t = 100$, 50, and 40 ns, respectively. For a particular system, the total number of formed clusters are divided into bins with each bin containing 25 carbon atoms. Clusters containing less than five carbon atoms are ignored. The different statistical distributions are modeled with gamma distribution functions[4] and the parameters for each distribution are given in the figure caption. A gamma distribution in a two-parameter family of continuous statistical distributions, is related to Poisson distributed events. The probability distribution function can be written as $P(x) = ((x^\alpha - 1)\exp(-x/\alpha)/\Gamma(\alpha)\theta^\alpha)$, with α and θ as the shape and scale parameters, and $\Gamma(\alpha)$ the usual gamma function.

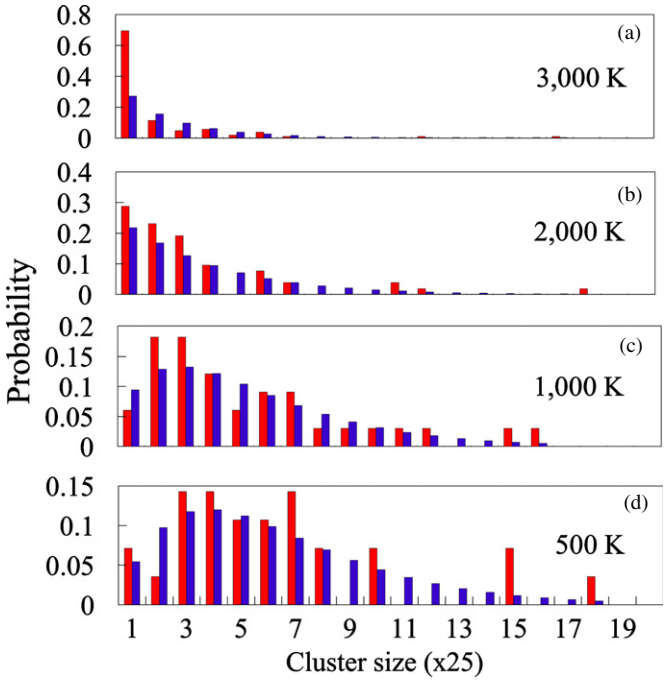

Figure 3. Probability distribution of carbon clusters (based on the atom numbers in each cluster). (a) Simulated and gamma (blue; $\alpha = 0.7571$ and $\theta = 2.5915$) probability distributions of obtained cluster sizes, when 4100 carbon atoms (atom density, $\rho = 4.0 \times 10^{-6}$ Å^{-3}) are simulated at $T = 3000$ K. Snapshot taken at $t = 40$ ns. (b) Simulated and gamma (blue; $\alpha = 1.0832$ and $\theta = 3.177804$) probability distributions of obtained cluster sizes, when 4100 carbon atoms (atom density, $\rho = 4.0 \times 10^{-6}$ Å^{-3}) are simulated at $T = 2000$ K. Snapshot taken at $t = 50$ ns. (c) Simulated and gamma (blue; $\alpha = 2.0007$ and $\theta = 2.6959$) probability distributions of formed cluster sizes with 4100 carbon atoms (atom density, $\rho = 4.0 \times 10^{-6}$ Å^{-3}) at $T = 1000$ K. Snapshot taken at $t = 100$ ns. (d) Simulated and gamma (blue; $\alpha = 2.3902$ and $\theta = 2.6447$) probability distributions of formed cluster sizes with 4100 carbon atoms (atom density, $\rho = 4.0 \times 10^{-6}$ Å^{-3}) at $T = 500$ K. Snapshot taken at $t = 200$ ns. Each bin contains 25 carbon atoms.

(A color version of this figure is available in the online journal.)

Figure 3(a), shows the probability distribution of carbon clusters at $T = 3000$ K (4100 C atoms and a simulation time of $t = 40$ ns). We find that carbon atoms form mainly small clusters along with a few curved and fullerene-type clusters. At high temperatures, large clusters are destabilized by the high thermal energy. Here, the entropy dominates over enthalpy in the Gibbs free energy of the system. The high formation probability of the very small clusters ($n_C < 20$) is confirmed by the probability distribution analysis in Figure 3(a). At $T = 2000$ K, although carbon atoms mainly form small clusters ($n_C \approx 35$), small graphene flakes and a few large curved clusters with five- and six-member rings (bowl shape) are observed along with chains molecules (as shown in Figure 3(b) with 4100 C atoms, sampled at $t = 50$ ns of simulations). At $T = 3000$ K and $T = 2000$ K, the carbon atoms are still in the gaseous phase (in which small clusters were mainly present) after 40 and 50 ns, respectively. It is also important to note that high temperatures are required to overcome the barrier that separates curved structures from flat structures.

[4] www.mathworld.wolfram.com/GammaDistribution.html

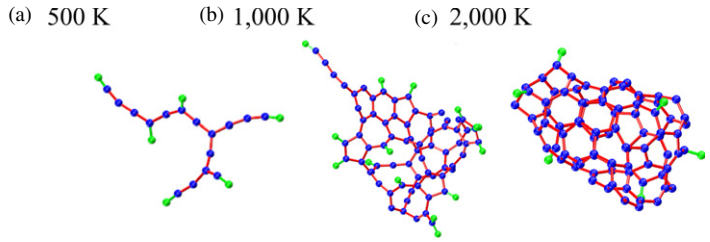

Figure 4. Formation of carbon–hydrogen clusters (the most dominant structures are shown; snapshots taken at $t = 200$ ns). We placed 256 carbon atoms and 256 hydrogen atoms in a cubic box ($500 \times 500 \times 500$ Å^3). (a) Short unsaturated chain and branched molecules, terminated with hydrogen atoms, are formed at $T = 500$ K. (b) Planar clusters, terminated with hydrogen atoms, are observed at $T = 1000$ K. (c) At $T = 2000$ K, fullerene-like clusters, with some hydrogen atoms attached to the surface, are found.

(A color version of this figure is available in the online journal.)

Next, we determine the probability distribution for 4100 C atoms (Figure 3(c)) and 10,000 C atoms (see the Appendix) at $T = 1000$ K, sampled at $t = 100$ ns. In this case, we observe that the most probable carbon clusters consist of $n_C \approx 75$ carbon atoms. As shown in Figure 3(d) with 4100 atoms (for 10,000 C atoms, see the Appendix) at $T = 500$ K, sampled at $t = 200$ ns, carbon clusters containing $n_C \approx 100$ carbon atoms are more likely to form. For 10,000 atoms at $T = 500$ K, sampled at $t = 200$ ns, the same probability distribution of carbon clusters is found. The maxima of the probability distribution also indicates the emergence of a "liquid phase" (in which relatively large clusters are present) at $T = 500$ K after $t = 200$ ns. During longer equilibration times, several small clusters can merge to form big clusters at low temperatures.

At low temperatures, carbon atoms initially form short chains and then several chains coalesce to form long chain molecules. Large cluster-type molecules with large member carbon rings emerge from several long chains. Eventually, these large clusters reorganize and form graphene-type sheets or bent clusters. At high temperatures, initially, short chain molecules/fragments are formed from carbon atoms, which then condense to form small clusters with relatively small member carbon rings. Eventually, these small clusters merge and form graphene or fullerene-type molecules.

3.4. Hydrogenation Process

In order to investigate the influence of the addition of hydrogen atoms on the structure of carbon cages/clusters, we simulate two systems where the ratio between carbon atoms and hydrogen atoms are 1:1 and 1:2, respectively. We also investigate the effect of concentration on the self-assembled structures by varying the atomic concentration. This aspect of the study is not directly relevant to ISM conditions, as the C:H ratio in the ISM is about 10^{-4}. The following simulations illustrate how the cluster growth is terminated when hydrogen atoms are introduced. For each study, after a short minimization, we simulate the cluster formation at different temperatures. Here, we notice the formation of alkene and other unsaturated carbon–hydrogen chain molecules along with small carbon clusters and hydrogen molecules. We observe that hydrogen atoms terminate the growth of big carbon clusters. At $T = 500$ K, small chains (terminated with hydrogen atoms) are predominantly found (Figure 4(a)). Planar clusters (Figure 4(b)), terminated by hydrogen atoms, are observed at $T = 1000$ K. Fullerene-type clusters are observed at $T = 2000$ K (few hydrogen atoms are bonded on the surface), as shown in Figure 4(c). We also observe vinyl-type polymers (not shown), in addition to linear alkyne chains. At low temperatures, both the C–H and C–C bond formations are favorable, but at high temperatures C–H bond formation is less favorable compared to C–C bonds due to high thermal fluctuation. Therefore, small hydrogen-terminated carbon chains are observed at low temperatures, while graphene to fullerene-type clusters are formed at high temperatures.

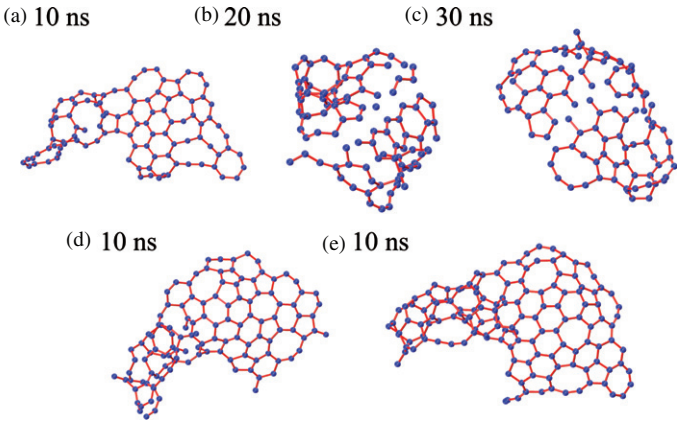

Figure 5. Carbon inflow at $T = 1750$ K. 100 carbon atoms were placed in a cubic box ($150 \times 150 \times 150$ Å^3). (a) Formation of a planar cluster with a few six- and five-member rings is observed; snapshot taken at $t = 10$ ns. (b) Bend cluster, with six- and five-member rings, is observed after $t = 20$ ns. (c) An additional bend structure, with only five- and six-member rings, is formed after $t = 30$ ns (note that some C–C bonds are missing for (b) and (c); this is due to the fact that some parts of these structures are in other periodic boxes and VMD (visualization software) cannot draw bonds in such situations). (d) Formation of planar cluster after $t = 10$ ns, where 20 carbon atoms are added after $t = 10$ ns simulation of 100 carbon atoms (a). (e) Formation of even bigger planar cluster after $t = 10$ ns, where another 20 carbon atoms are added after $t = 10$ ns simulation of 120 carbon atoms (d).

(A color version of this figure is available in the online journal.)

3.5. Carbon Inflow: Non-equilibrium Nucleation

While in a chemical steady-state condition the significant curvature of graphitic sheets that leads to spontaneous folding may not occur at certain low temperatures, the inflow of carbon material could facilitate an approach to additional equilibria leading to curved carbon clusters and finally to fullerene formation. This situation better resembles astrophysical environments. The process of carbon inflow in ISM may not necessarily follow a Boltzmann distribution. We intend to understand how the carbon inflow influences the formation process. To this end, we perform a simulation with 100 gaseous carbon atoms in a 150 Å^3 box (atom density, $\rho = 2.96 \times 10^{-5}$ Å^{-3}) at $T = 1750$ K (all other conditions are the same as described above). After equilibrating for $t = 10$ ns, we save the coordinates of all atoms

at the last frame and add another 20 carbon atoms, keeping the box size fixed (total carbon atoms = 120; atom density, $\rho = 3.55 \times 10^{-5}$ Å^{-3}). After minimization, we simulate for another $t = 10$ ns equilibrating at $T = 1750$ K and save the coordinates of all atoms of the last frame and repeat the process one more time (total carbon atoms = 140; atom density, $\rho = 4.15 \times 10^{-5}$ Å^{-3}).

As shown in Figure 5(a), we observe that a planar cluster with a few six- and five-member rings forms after $t = 10$ ns. Within $t = 20$ ns, the formation of a bend structure is observed with more six- and five-member rings (Figure 5(b)), and after $t = 30$ ns, curved structures are observed in which almost all carbon atoms form six- or five-member rings (Figure 5(c)). When we add 20 carbon atoms to the structure in Figure 5(a) and simulate for another $t = 10$ ns, we observe more planar structures compared to Figure 5(b), as shown in Figure 5(d). The added carbon atoms form bonds with the edge carbon atoms of Figure 5(a) and tend to create six-member rings. When we add another 20 carbon atoms to Figure 5(d), we observe more planar structure (Figure 5(e)) compared to Figure 5(c), as the added carbon atoms again form bonds with the edge carbon atoms of Figure 5(d) and create more six-member rings.

4. CONCLUSION

We study conditions under which large carbon structures form and stabilize in the gas phase in interstellar space by using reactive MD simulations. The formation mechanisms of the large clusters and graphene-type structures are investigated through a series of MD simulations, and the influence of temperature and particle density on the shape of structures is studied. It is found that at high temperature ($T = 2000$–3000 K), fullerene-type clusters are obtained, whereas at relatively low temperatures, graphene-type sheets and long chain molecules/structures are synthesized. Analytical expressions for the formation of small chain molecules can be used to predict the time scale for the formation of nanostructures in the ISM. We determine the probability distributions of cluster sizes at different temperatures and the initial C atom number and compare them with gamma distributions. The effect of adding hydrogen atoms to the structures of carbon atoms is also studied. At high temperatures, fullerene-type clusters are found whereas short and branched chain molecules, terminated with hydrogen atoms, are observed at low temperatures. When there is a higher density of hydrogen atoms, we find that small unsaturated carbon chains are formed. When the concentration of hydrogen is relatively low, a graphene-type sheet (terminated by hydrogen atoms) and small cluster are observed. Finally, we simulate the self-assembly of carbon structures, in non-equilibrium conditions of periodic carbon inflow, resembling astrophysical conditions.

These studies help to better understand the tenuous gaseous conditions in ISM during the synthesis of large carbon structures. We find that in the extreme conditions presented by low temperature and low density, system entropy plays a significant role in hindering synthesis and destabilizing large carbon structures. In future studies, we intend to investigate how dynamical quantum tunneling and stellar irradiation can lead to new pathways to carbon cluster formation. UV irradiation and shock waves can ionize the gas and significantly affect molecular synthesis in the ISM. Quantum chemical calculations are necessary to address and understand the ionization process. When the quantum chemical calculations are limited by the system size, classical (semi-empirical) methods with improved force fields can be used to understand the nucleation process.

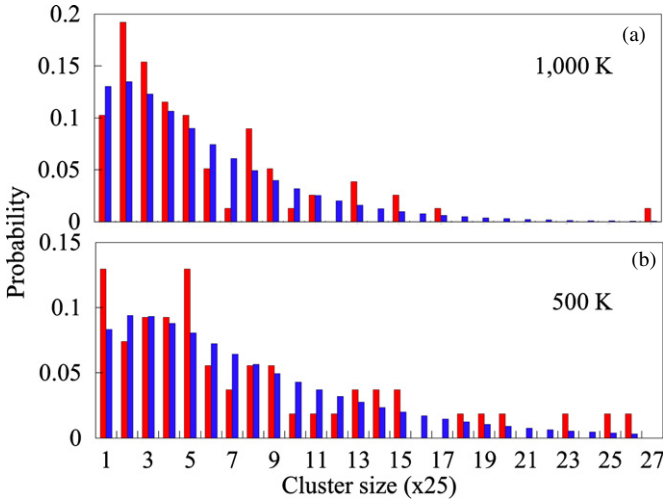

Figure 6. Probability distribution of carbon clusters (based on atom numbers in each cluster). (a) Simulated and gamma (blue; $\alpha = 1.4441$ and $\theta = 5.3347$) probability distributions of cluster sizes with 10,000 carbon atoms (atom density, $\rho = 4.0 \times 10^{-6}$ Å^{-3}) at $T = 500$ K. The snapshots are taken at 200 ns. (b) Simulated and gamma (blue; $\alpha = 1.4342$ and $\theta = 3.7367$) probability distributions of cluster sizes, with 10,000 carbon atoms (atom density, $\rho = 4.0 \times 10^{-6}$ Å^{-3}) at 1000 K. The snapshots are taken at 100 ns. Each bin contains 25 carbon atoms.

(A color version of this figure is available in the online journal.)

N.P. acknowledges support from the SAO Fellowship. The authors are grateful for the allocation of computer time on the Kraken Cluster at the NSF-XSEDE and Odyssey Clusters at Harvard University where parts of the simulations were conducted. Financial support was provided by a Smithsonian Grand Challenges Award.

APPENDIX

SIZE DISTRIBUTIONS OF CARBON CLUSTERS

The cluster size probability distributions (based on the C atom number) are determined for a system with 10,000 carbon atoms (carbon density, $\rho = 4.0 \times 10^{-6}$ Å^{-3} in gas phase at $T =$ 1000, and 500 K). Figure 6(a), shows the probability distribution of carbon clusters at $T = 1000$ K (with a simulation time of $t = 100$ ns). We find that intermediate sized clusters are mainly formed ($n_C = 50$–100 carbon atoms). As discussed, at $T = 500$ K, large clusters can be stabilized. The high formation probability of the large clusters ($n_C \geqslant 100$) at $T = 500$ K is confirmed by the probability distribution analysis in Figure 6(b). The maxima of the probability distribution also indicate the emergence of a "liquid phase" (in which relatively large clusters are present) at $T = 500$ K after $t = 200$ ns.

REFERENCES

Allamandolla, L. J., Tilenes, A. G. G. M., & Barker, J. R. 1985, ApJL, 290, L25
Belloche, A., Menten, K. M., Comito, C., et al. 2008, A&A, 482, 179
Berné, O., & Tielens, A. G. G. M. 2012, PNAS, 109, 401
Botta, O., & Bada, J. L. 2002, SGeo, 23, 411
Bradley, J., Dai, Z. R., Erni, R., et al. 2005, Sci, 307, 244
Brenner, D. W. 1990, PhRvB, 42, 9458
Cami, J., Bernard-Salas, J., Peeters, E., & Malek, S. E. 2010, Sci, 329, 1180
Cronin, J. R., & Chang, S. 1993, in NATO ASI Ser. 416, The Chemistry of Life's Origins, ed. J. M. Greenberg, C. X. Mendoza-Gomez, & V. Pirronello (Dordrecht: Kluwer), 209
Duley, W. W. 2006, FaDi, 133, 415
Eberlein, T., Bangert, U., Nair, R. R., et al. 2008, PhRvB, 77, 233406
Ehrenfreund, P., & Sephton, M. A. 2006, FaDi, 133, 277

Friberg, P., Hjalmarson, A., Madden, S. C., & Irvine, W. M. 1988, A&A, 195, 281
Garrod, R. T., & Herbst, E. 2006, A&A, 457, 927
Gibb, E. L., Whittet, D. C. B., Boogert, A. C. A., & Tielens, A. G. G. M. 2004, ApJS, 151, 35
Herbst, E., & van Dishoeck, E. F. 2009, ARA&A, 47, 427
Hollis, J. M., Lovas, F. J., & Jewell, P. R. 2000, ApJL, 540, L107
Hollis, J. M., Lovas, F. J., Remijan, A. J., et al. 2006, ApJL, 643, L25
Humphrey, W., Dalke, A., & Schulten, K. 1996, J. Mol. Graph., 14, 33
Irle, S., Zheng, G., Elstner, M., & Morokuma, K. 2003, NanoL, 3, 1657
Irle, S., Zheng, G., Wang, Z., & Morokuma, K. 2006, JPCB, 110, 14531
Irvine, W. M., Goldsmith, P. F., & Hjalmarson, A. A. 1987, in Interstellar Processes, ed. D. J. Hollenbach & H. A. Thronson (Dordrecht: Reidel), 561
Liader, K. J., Meiser, J. H., & Sanctuary, B. C. 2003, Physical Chemistry (4th ed.; Boston: Houghton Mifflin)
Lozovik, Y. E., & Popov, A. M. 1997, PhyU, 40, 717
Marcelino, N., Cernicharo, J., Agundez, M., et al. 2007, ApJL, 665, L127
Ohishi, M., & Kaifu, N. 1998, FaDi, 109, 205
Parker, D. S. N., Zhang, F., Kim, Y. S., et al. 2012, PNAS, 109, 53
Plimpton, S. J. 1995, JCoPh, 117, 1
Ricks, A. M., Douberly, G. E., & Duncan, M. A. 2009, ApJ, 702, 301
Salama, F. 2008, in IAU Symp. 251, Organic Matter in Space, ed. S. Kwok & S. Sanford (Cambridge: Cambridge Univ. Press), 357
Salama, F., Galazutdinov, G. A., Krelowski, J., Allamandola, L. J., & Musaev, F. A. 1999, ApJ, 526, 265
Schutte, W. A. 1996, in The Cosmic Dust Connection, ed. J. M. Greenberg (Dordrecht: Reidel), 1
Sellgren, K., Werner, M. W., Ingalls, J. G., et al. 2010, ApJL, 722, L54
Servantie, J., & Gaspard, P. 2003, PhRvL, 91, 185503
Spencer, M. K., Hammond, M. R., & Zare, R. N. 2008, PNAS, 105, 18096
Stuart, S. J., Tutein, A. B., & Harrison, J. A. 2000, JChPh, 112, 6472
Tielens, A. G. G. M. 2008, ARA&A, 46, 289
Winnewisser, G., & Kramer, C. 1999, SSRv, 90, 181
Witt, A. N., Schild, R. E., & Kraiman, J. B. 1984, ApJ, 281, 708